Ultralow Velocity Zone at the Core-Mantle Boundary

Edward J. Garnero

Berkeley Seismological Laboratory, University of California, Berkeley, CA

Justin Revenaugh, Quentin Williams, and Thorne Lay

Institute of Tectonics and Earth Sciences Department, University of California, Santa Cruz, CA

Louise H. Kellogg

Department of Geology, University of California, Davis, CA

Accumulating seismic evidence for a laterally varying thin ultralow velocity zone (ULVZ) at the base of the mantle is summarized, and shown to have far reaching implications. Anomalous *SPdKS* delays and amplitudes, and precursory energy to *PcP*, *ScP*, and *PKP* require seismic velocity reductions of at least 10% in some regions of the boundary layer. Estimates of ULVZ thickness depend on poorly constrained parameters such as the shear velocity and density, but it is likely less than 20-40 kilometers, where present. The most probable cause of the ULVZ is partial melting of the lowermost mantle, with chemical heterogeneity and dynamic effects playing an important role as well. Strong spatial correlations between regions with detected ULVZ zones and surface positions of buoyancy flux-weighted hot spots, as well as between regions lacking a detectable ULVZ and areas of accumulated subducted material, suggest a direct relationship between the top and bottom boundary layers of the mantle, strongly supporting the idea of circulation between the upper and lower mantle.

1. INTRODUCTION

Over the past several decades, deep Earth research has yielded first-order information on properties of the core-mantle boundary (CMB) region, such as large-scale lateral variations and strong radial gradients and discontinuities in mantle seismic velocities, and inferred large-scale flow properties (see *Loper and Lay* [1995] for a review). More recently, details of structure in the lowermost 200-300 kilometers of the mantle (the D″ region) have emerged, revealing the presence of seismic shear wave anisotropy, coherent small scale scattering, thin low-velocity basal layering, and probable ongoing chemical reactions between the solid silicate mantle and liquid iron-alloy core; the emerging picture of the lowermost mantle is as complex as for the Earth's lithosphere, with both regions being dynamic thermal and chemical boundary layers [see references contained in *Loper and Lay*, 1995; *Wysession*, 1996a; *Wysession et al.*, 1997; *Lay et al.*, 1998].

Resolving structure of the Earth's boundary layers at the top and bottom of the mantle is crucial to understanding large scale mantle flow, since the dynamics of the boundary layers is expected to be closely coupled to upwelling and downwelling motions of the convective system. Determining the configuration of seismic velocity layering, heterogeneity and anisotropy provides direct information on the thermal and chemical processes in both boundary layers.

Recently, evidence for a laterally varying thin layer at the base of the mantle with large velocity reductions has been discovered using different methods [e.g., *Mori and*

The Core-Mantle Boundary Region
Geodynamics 28

Helmberger, 1995; *Garnero and Helmberger*, 1996; *Vidale and Hedlin*, 1998]. This ultralow velocity zone (ULVZ) has been imaged as having variable thickness (5-40 kilometers) and *P* wave velocity reductions of at least 10%. Explanation of the ULVZ as a result of partial melt [*Williams and Garnero*, 1996; *Holland and Ahrens*, 1997; *Revenaugh and Meyer*, 1997; *Vidale and Hedlin*, 1998; *Wen and Helmberger*, 1998a] implies approximately a 3:1 reduction in *S* wave velocities (V_S) compared to *P* wave velocities (V_P) in the layer (thus at least a 30% shear velocity reduction). Other possible explanations for the ULVZ, such as chemical heterogeneity, have different implications for shear velocity reductions. Better understanding of this layer of ultralow velocities in relation to lower mantle mineralogy (e.g., composition and state), mantle dynamics (e.g., small and large scale circulation, including plumes and downwellings), core dynamics (possible influences on magnetic reversals and the geodynamo) and other seismic phenomena (e.g., scattering, anisotropy) are the focus of this paper. In what follows, we first review relevant studies of lower mantle *P* waves, since ULVZ work to date has primarily imaged *P* wave velocity structure, followed by a detailed discussion of present seismic methods used for ULVZ imaging (and their uncertainties). Finally, mineral physics and geodynamics considerations demonstrate far reaching implications. Diverse observables at the Earth's surface such as hot spots and subduction zones, and observed magnetic field reversal paths, show strong spatial correlations with the ULVZ distribution.

2. LOWER MANTLE *P* VELOCITY STRUCTURE

Patterns of *P* wave velocity heterogeneity in the lowermost few hundred kilometers of the mantle have been imaged globally at scale lengths of 3000-5000 kilometers and greater [e.g., *Dziewonski*, 1984; *Inoue et al.*, 1990; *Pulliam et al.*, 1993; *Wysession*, 1996b; *Sylvander et al.*, 1997], as well as locally at intermediate to short wavelength (≈ 3000 kilometers to less than 100 kilometers) [e.g., *Young and Lay*, 1989; *Wysession and Okal*, 1989; *Weber and Körnig*, 1990; *Weber*, 1993; *Souriau and Poupinet*, 1994; *Krüger et al.*, 1995; *Wysession et al.*, 1995; *Sylvander and Souriau*, 1996; *Scherbaum et al.*, 1997]. Many studies use seismic waves and methods that average the radial V_P structure over a minimum of several hundred kilometers, i.e., throughout D″ (e.g., travel time analyses of *PcP*, *PKP*, and diffracted *P* waves, *Pd*) and thus do not resolve the velocity structure in the lowermost few tens of kilometers of the mantle where the ULVZ has been detected. Thus any strong velocity variations in an unresolved thin transition zone structure may have been erroneously mapped into models of V_P heterogeneity or velocity gradients in the lowermost few hundred kilometers of the mantle. For example, *Song and Helmberger* [1995] argued for moderately reduced V_P in the lowermost 200-300 kilometers of the mantle to explain observed separations of the DF and AB branches of *PKP* phases at large distances. Alternatively, the data may be explained by stronger velocity reductions in the lowermost 5-40 kilometers of the mantle.

Some studies have noted that the presence of a thin heterogeneous mantle basal layer helps in explaining various seismic observations, even if the thin zone is not uniquely resolved by the data under consideration. For example, in an analysis of *PcP*, *PKP* and *PKKP* arrival times (as recorded by the International Seismological Centre), *Doornbos and Hilton* [1989] considered a model parameterization with a 20 kilometers thick layer at the CMB. While noting a strong trade-off between the velocity reduction and thickness of the layer, they preferred a layer having a 20% reduction in V_P. More recently, it has been shown that a ULVZ basal layer can explain anomalous *PKP* AB-BC separations [see *Sylvander and Souriau*, 1996]. Also, perturbations in *Pd* times have been attributed to a basal layer with ±10% V_P heterogeneity [*Sylvander et al.*, 1997]. As we discuss below, the presence of a thin transition zone can cause detectable waveform (and associated travel time) perturbations in particular long period and broadband seismic arrivals, as well as producing additional precursory arrivals in short period *P* wave recordings [e.g., *Wysession*, 1996b; *Scherbaum et al.*, 1997; *Revenaugh and Meyer*, 1997]. Thus it is possible to directly establish the presence and parameters of a thin basal layer rather than inferring it from a parameterized tomographic inversion.

3. SEISMIC IMAGING OF ULTRALOW VELOCITY ZONES

3.1 Previous Work

Detailed waveform modeling studies have revealed evidence for a laterally varying low velocity layer right above the CMB. A map of lowermost mantle regions that have been previously investigated for this ULVZ structure is displayed in Figure 1. Fresnel zones are shown, and cover roughly 44% of the CMB surface area. Regions having a ULVZ are denoted by light shading, and those showing no evidence for a ULVZ have dark shading (recognizing that the ULVZ may be present, but too thin to detect in these areas). The Fresnel zones provide an estimate of the region which kinematically can contribute to the first quarter wavelength of the seismic arrivals used to map the ULVZ. The actual wavefield involves lateral averaging over these dimensions, however, it is important to keep in mind that variations at scale lengths smaller than the Fresnel zone are not precluded or constrainable, and in fact may significantly

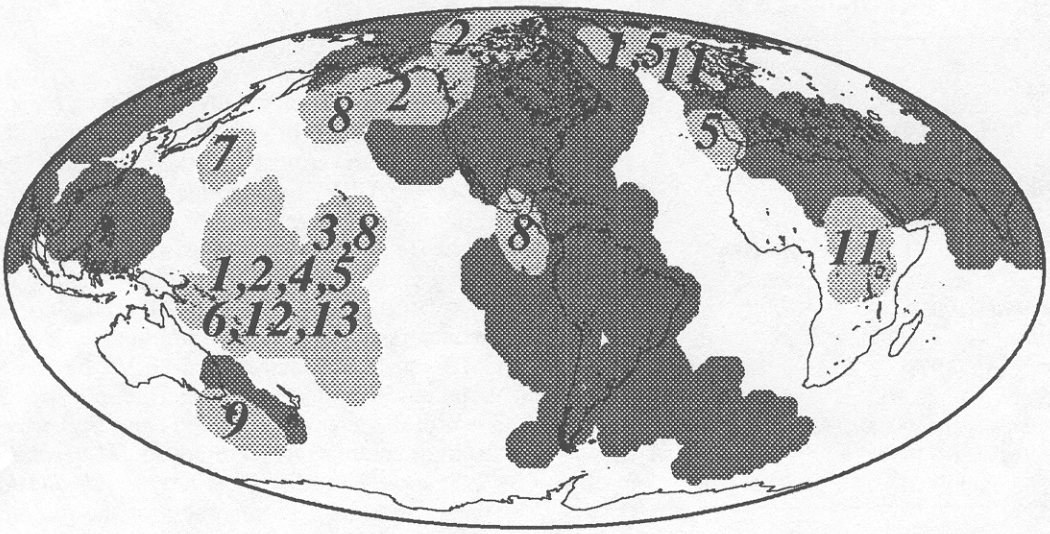

Figure 1. Shaded areas correspond to CMB regions investigated for ULVZ structure. CMB Fresnel zones are shown. Lighter shading corresponds to regions where evidence for ULVZ structure has been found, the numbers correspond to specific studies, as listed in Table 1. The darker shading indicates CMB regions lacking evidence for ULVZ structure, and is based on data in studies 2, 5, and 9 in Table 1 (see text for more details).

contribute to any observed anomaly. The large ULVZ patch in the southwest Pacific (Figure 1), for example, may contain lateral variations within it, and any single one-dimensional model for the region applies only in an average sense. Nonetheless, the Fresnel zone representation provides a first-order characterization of spatial extent of detectable ULVZ at a lateral scale that allows comparisons with other geophysical observations.

The ULVZ regions are numbered corresponding to the studies listed in Table 1. The table also lists the seismic phases and data type used. Since seismology is the most direct means for investigating this structure, we discuss the different seismic phases that constrain the ULVZ characteristics.

3.2 SPdKS Data

The seismic phase *SPdKS* is an *SKS* wave with additional segments of mantle-side CMB *P* wave diffraction (*Pd*) at the *SKS* core entry and exit locations (Figure 2a). The nomenclature "*SPdKS*" is generically used to represent a composite of seismic energy having contributions from *(i)* an *SKS* wave with a segment of *Pd* on the source-side of the wavepath (i.e., *SPdKS*, Figure 2b); *(ii)* an *SKS* wave with a segment of *Pd* on the receiver-side of the wavepath (i.e., *SKPdS*); *(iii)* various combinations of *(i)* and *(ii)*, see *Choy* [1975] and *Garnero et al.* [1993]; and *(iv)* if a ULVZ is present, energy from an *SV*-to-*P* mode-conversion at the CMB followed by an internally reflected *P* wave ("*SpKS*", Figure 2b, see also *Helmberger et al.* [1996]). Unless specifically indicated otherwise, the term "*SPdKS*" refers to the composite energy arrival. We note that our synthetic modeling of *SPdKS* incorporates all of the separate contributions to the arrival.

SPdKS wavepaths through the lower mantle are very close to *SKS*, typically separated by less than 200 kilometers at the CMB [*Garnero et al.*, 1993]. Thus, referencing *SPdKS* to *SKS* in time and amplitude eliminates source dependence and provides sensitivity to very localized CMB regions. This is especially true when using *SPdKS* data with short *Pd* segments, i.e., at distances close to the inception of *SPdKS* (near 108°, a model dependent distance). It is noteworthy that anomalously low *P* velocities can affect amplitude ratios involving *SKS* [*Silver and Bina*, 1993] since the amount of *SKS* energy transformed into *SPdKS* arrivals is a model dependent phenomena [*Helmberger et al.*, 1996].

An uncertainty in *SPdKS* modeling is that the composite energy arriving as *SPdKS* has *Pd* contributions from possibly differing CMB structures on the source and receiver sides of the wavepath. In this case, however, the energy contributing to *SPdKS* from the more anomalous of the two ULVZ regions will dominate the arrival, due to more effective SV-to-P mode conversions in the ULVZ (e.g., *SpKS*) and better trapping of *Pd* (of *SPdKS*) energy in the boundary layer. Additional information, such as criss-crossing geometries, is needed to resolve the uncertainty of which side of the wavepath contains the ULVZ anomaly (as demonstrated by *Garnero and Helmberger* [1996] for the case of the central Pacific ULVZ).

Table 1. Past ULVZ studies

#	Study	Seismic Phase	Data Type[a]
1	*Garnero et al.* [1993]	*SPdKS*	LP
2	*Garnero, Helmberger* [1995]	*SPdKS*	LP
3	*Mori, Helmberger* [1995]	*PcP*	SPA
4	*Vidale et al.* [1995]	*ScP*	SPA,BB
5	*Garnero, Helmberger* [1996]	*SPdKS*	LP
6	*Helmberger et al.* [1996]	*SPdKS*	LP,SPW
7	*Fischer et al.* [1996]	*SPdKS*	BB
8	*Revenaugh, Meyer* [1997]	*PcP*	SPA
9	*Williams et al.* [1998]	*SPdKS,PcP*	LP,SPA
10	*Helmberger et al.* [1998]	*SPdKS*	LP
11	*Wen, Helmberger* [1998b]	*SPdKS*	LP
12	*Wen, Helmberger* [1998a]	*PKP* prec.	BB
13	*Vidale, Hedlin* [1998]	*PKP* prec.	SPA,BB

[a] LP, Long period WWSSN data; SPW, Short period WWSSN data; SPA, short period array data; BB broadband data

The threshold for detection of ULVZ structure using *SPdKS* data is dependent on both the wavelength of seismic data and ULVZ properties. For a ULVZ with V_P and V_S reductions of 10% and 30%, respectively, layer thicknesses greater than 3-5 kilometers are detectable with long period World Wide Standardized Seismographic Network (WWSSN) data. Smaller ULVZ thicknesses are detectable with broadband data and/or larger velocity reductions in the layer. Thus the areas with dark shading in Figure 1, many of which are sampled by WWSSN data, may actually have an undetectably thin ULVZ (< 3-5 kilometers).

Data that sample anomalous ULVZ structure beneath the southwest Pacific and Iceland are displayed in Figure 3. The first arrival is *SKS*, and the secondary pulse, appearing as a shoulder on *SKS* at smaller distances (e.g., 110°), is *SPdKS*. Predictions for the delay time of the peak of *SPdKS* relative to *SKS* for the Preliminary Reference Earth Model (PREM) [*Dziewonski and Anderson*, 1981] are indicated by a dashed line (as measured from synthetic seismograms generated by the reflectivity method [e.g., see *Fuchs and Müller*, 1971]). Readily apparent are observed *SPdKS* delays of up to 5 s relative to *SKS*. These delays are often accompanied with anomalously large *SPdKS* amplitudes [see *Garnero and Helmberger*, 1998]. Waveforms with particularly large and delayed *SPdKS* are indicated by small filled circles. The observed *SPdKS* peaks arrive well after the PREM prediction (dashed line). A dotted line which fits the average of the anomalous *SPdKS* arrivals is delayed by several seconds relative to PREM, with large variations about this trend indicating the presence of strong small scale lateral variations [*Garnero and Helmberger*, 1996, 1998].

3.3 PcP and ScP Data

ScP and *PcP* waveforms (typically having measurements made relative to direct *P*, see Figure 2a) are also effective probes for ULVZ structure. Any large contrast in lowermost mantle properties (such as at the top of the ULVZ) can reflect significant seismic energy, resulting in a precursor to core-reflected *ScP* and *PcP* waves (Figure 2c and 2d). Also, *ScP* can have precursory energy from an *S*-to-*P* mode conversion in down-going *S* energy encountering the top of the ULVZ (see Figure 2c). Precursors to *ScP* waves sampling the southwest Pacific CMB can be explained by a ULVZ having strong lateral variations [*Vidale et al.*, 1995]. Short-period array data are useful for analysis of *PcP* and *ScP* waveforms when stacking methods are employed [*Mori and Helmberger*, 1995; *Vidale et al.*, 1995; *Revenaugh and Meyer*, 1997]. Also, issues such as sharpness of the discontinuity at the top of the ULVZ can be addressed with short-period data.

Unlike *SPdKS* phase anomalies which can be observed in individual seismograms, short-period precursors to *PcP* reflected from the top of the ULVZ can only be seen in stacks of many records. Figure 4 is a profile of stacked traces of nearly 1500 recordings from the Northern and Southern California Seismic Networks for nearly 100 intermediate and deep earthquakes in the Tonga subduction zone. Prior to stacking, the records were deconvolved using source-specific average *P* waveforms on an event-by-event basis. The stack combines records within small (0.4 s) calculated *PcP-P* delay time bins; the total range of delay times corresponds to a distance range

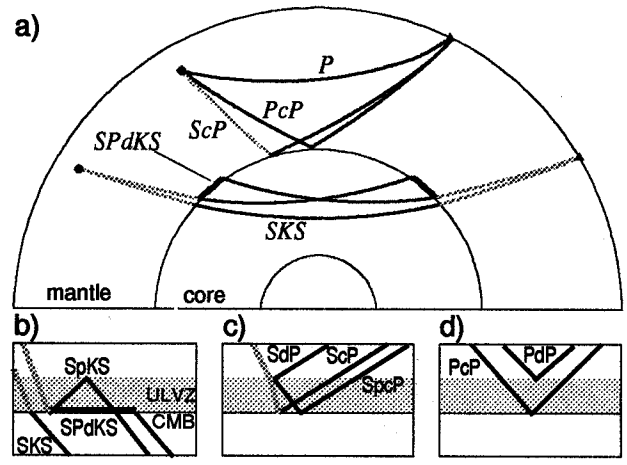

Figure 2. (a) Cross-section of the Earth showing geometrical ray paths for the seismic phases *SKS* and *SPdKS* at 120°, and *PcP*, *ScP*, and *P* at 60°. *S* wave particle motions are indicated by gray lines, *P* wave motion by black lines. Zoom in at the CMB is shown for (b) *SPdKS*, (c) *ScP*, and (d) *PcP*, displaying additional arrivals due to the ULVZ.

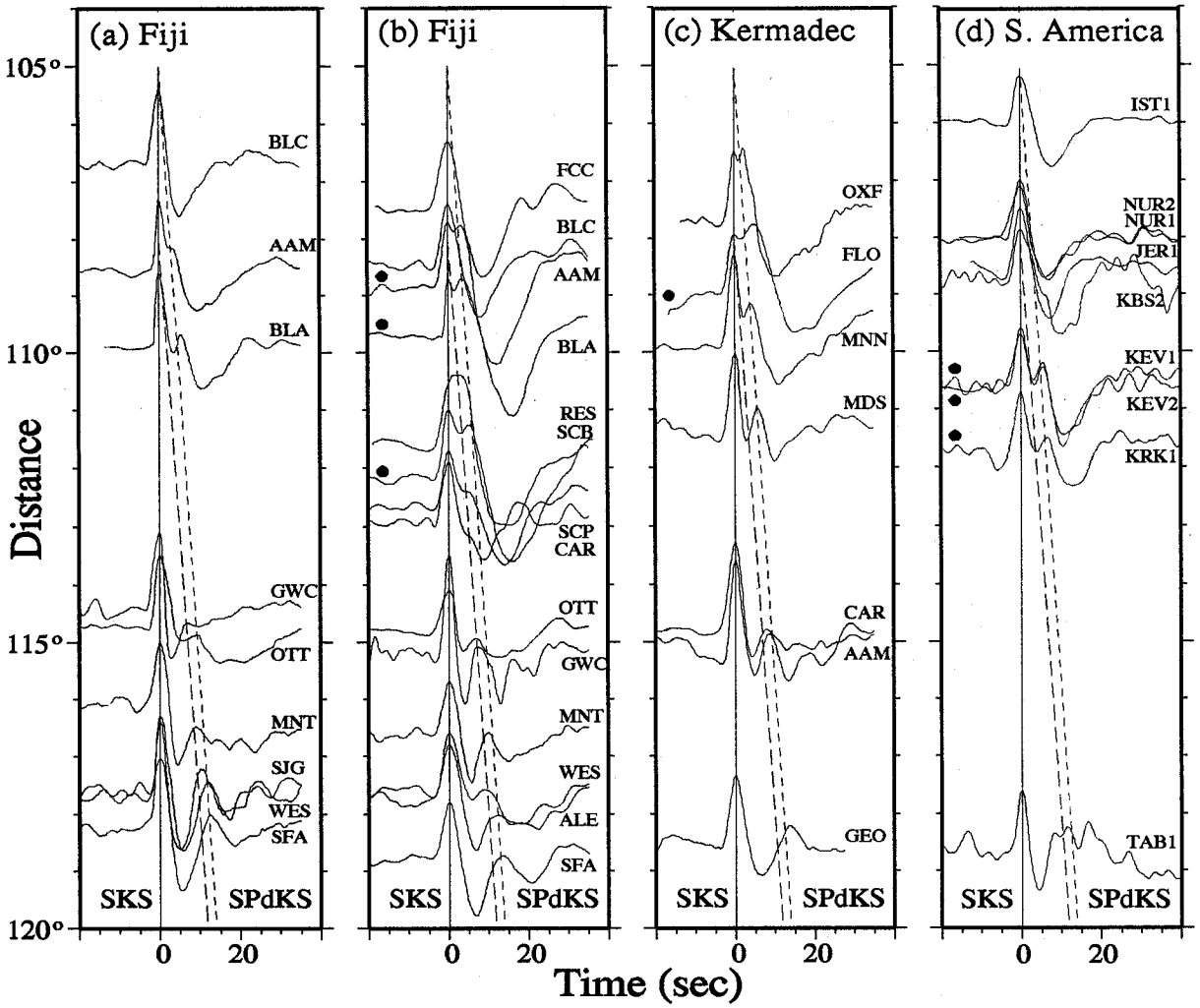

Figure 3. Longitudinal component long-period WWSSN recordings of *SKS* and *SPdKS*, the first and second arrivals, respectively. The first (solid) and second (dashed) lines correspond to *SKS* and *SPdKS* predictions, respectively, of the PREM model. The third small dashed line is drawn to aid in identifying delayed *SPdKS* peaks. Many records show extreme *SPdKS* time and amplitude anomalies, and are indicated by dots on the left of the trace. All times and amplitudes are normalized to SKS.

of ≈78° to 90°. A standard reference Earth model is used to predict the differential times and data are aligned on actual *P* arrivals. The asymmetry of the *PcP* wavelets (relative to the stacked *P* signals) is evidence of a reverse-polarity precursor, referred to as *PdP*.

A curved-wavefront stacking algorithm using 5509 seismograms was computed for events in the Tonga-Fiji subduction complex for target reflectors spaced every two kilometers in depth in the lowermost mantle [*Revenaugh and Meyer*, 1997]. Figure 5a displays the result as computed *PdP*/*P* stack amplitude ratio versus the corresponding reflector depth relative to the CMB. In this case, a single midpoint bin was used, ignoring structural variation near the bounce points of *PdP*. Nonetheless, a peak identified as *PcP* is non-zero well above the 95% confidence level, as is a precursory (shallower) trough that *Revenaugh and Meyer* [1997] associate with reverse-polarity reflection from a discontinuity approximately 16 kilometers above the CMB. (Delay of *PcP* due to the presence of a ULVZ, should be manifested as a reflector below the CMB in such a representation.) Comparison with a synthetic data stack illustrates the need for a second arrival. Although the stacked synthetic waveform is slightly asymmetric, the magnitude of the secondary shallow trough is much less than observed. It is not possible to mimic the trough

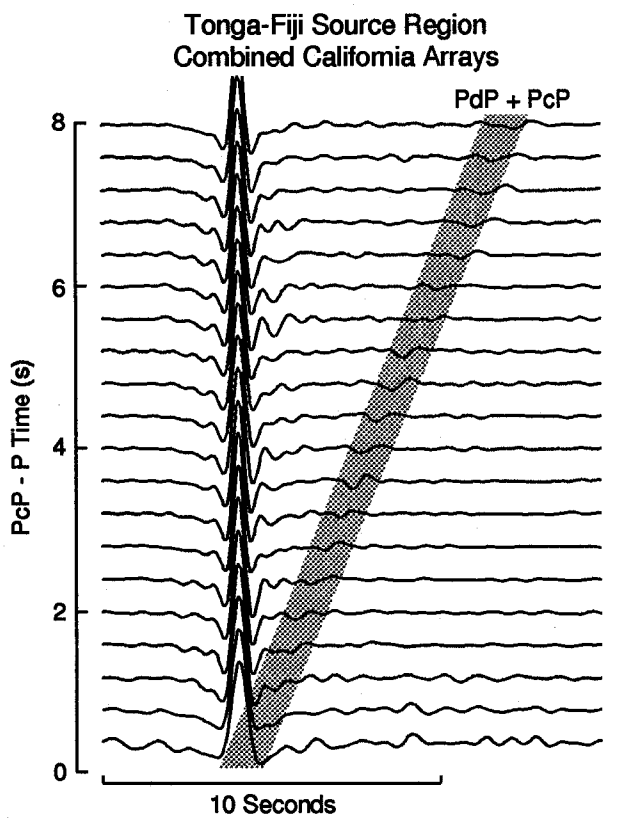

Figure 4. Stacked seismograms of Tonga-Fiji earthquakes recorded by the combined California regional arrays. *P* is the dominant signal. *PcP* appears as a small positive peak following *P* by the delay time shown on the left-hand axis (see shaded area). A small negative polarity precursor to *PcP* is apparent (*PdP*). The asymmetry of the *PcP* waveform relative to *P* is evidence of a low-amplitude, reverse polarity precursor to PcP, interpreted as a reflection from the top of the ULVZ.

simply by summing variably delayed *PcP* phases, i.e., the stack cannot be adequately modeled without a reversed polarity precursor to *PcP*, in accord with *Mori and Helmberger* [1995].

Figure 5b shows the aligned bin stacks of the same source area. Bins measuring 3° on a side were tiled over the region of densest midpoint coverage. The composite stack consists of 5 adjacent bins and 4217 seismograms. Peak amplitude depths range from 27 to 11 kilometers below the CMB in the five bin stacks, signifying a delayed *PcP* arrival and lower-than-average velocities in D″. The peak aligned stack amplitude of *PcP* and *PdP* is increased over that of Figure 5a and there is noticeable compaction of the stack peaks, signifying the reduction in travel time variability obtained by binning.

The mean reflector depth, reflection coefficient and remaining travel time variability of *PcP* and its precursor *PdP* were estimated by Monte Carlo methods with synthetic data stacks. Models were accepted if the observed minus predicted stack resulted in a 80% or greater variance reduction, a value chosen with reference to the bootstrap-derived confidence intervals. For the stacks in Figures 5a and 5b, all acceptable models have reversed polarity *PdP* (i.e., opposite of *P* and *PcP*). The amplitude of *PdP* relative to *P* can be used to bound acceptable velocity and density contrasts of the reflector. A grid search was conducted over shear velocity, compressional velocity, and density perturbations, computing a mean reflection coefficient ($\bar{R}_{PdP}$) for each perturbation triplet by matching the ray-parameter distribution of data. $\bar{R}_{PdP}$ predictions within 1.5 times the observed range of *PdP* reflection strengths were accepted. A further constraint, that the average *PcP* reflection coefficient be positive and less than 0.4, was included. The upper limit (0.4) is 3 times the largest accepted Monte Carlo value.

We find that both shear and compressional velocities must drop across the layer to produce the observed reversed polarity reflections (Figure 6). Furthermore, we observe a ≈3:1 ratio of shear to compressional velocity decrease in the model solution space. Density is relatively unimportant unless allowed to vary greatly (> 15%), in which case certain trade-offs exist as discussed in the next section. Here we present results for density perturbations less than ±10%. We explored the effects of a diffuse top of the ULVZ by calculating the acceptable velocity perturbations for a 5 kilometer transition zone. The effect of the broadened transition is to increase the

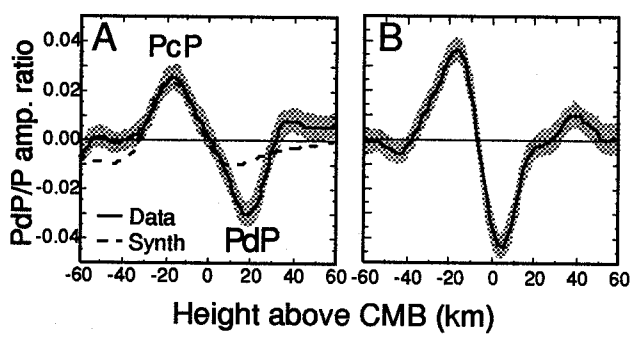

Figure 5. (a) Curved wavefront stack of observed (solid line) and synthetic (dashed line) *PdP-PcP* data for Fiji-Tonga events. Amplitudes normalized to *P*. Gray shading denotes 95% confidence intervals of the data stack. Synthetic stack contains only *P* and *PcP* arrivals and fails to match the precursory downswing to the *PcP* peak centered at -20 kilometers (negative depths imply slow lowermost mantle and a delayed *PcP* arrival, and should not be construed as CMB displacements). (b) As in (a) except data were separately stacked in small bounce point bins and aligned before stacking [see *Revenaugh and Meyer*, 1997].

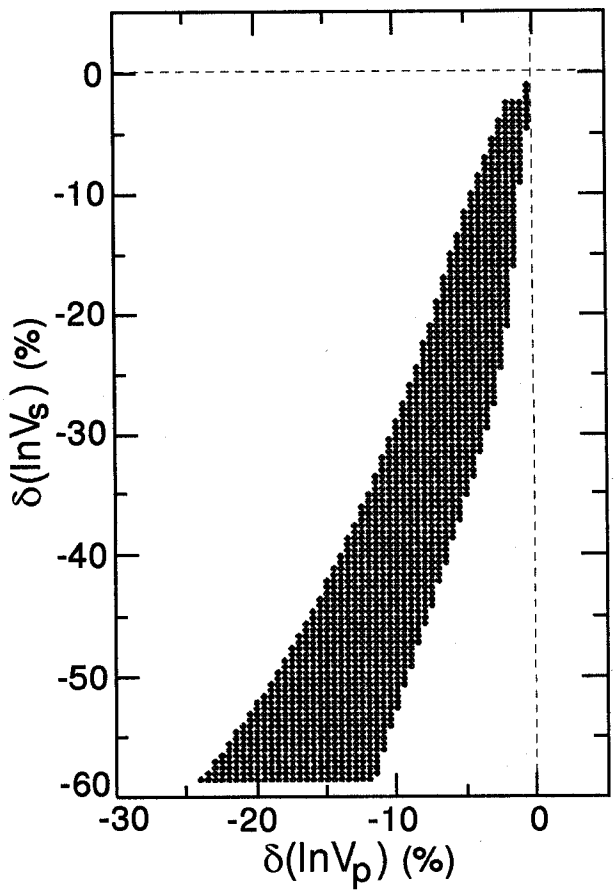

Figure 6. Acceptable velocity variations across an assumed first-order discontinuity responsible for the *PdP* precursor to *PcP* for Fiji-Tonga events. Negative values signify a velocity decrease across the discontinuity. All acceptable models have large V_S decreases. [After *Revenaugh and Meyer*, 1997].

magnitude of the minimum acceptable velocity reductions (i.e., greater velocity reduction) and to increase the range of acceptable models at greater velocity decrease, but the near 3:1 ratio of shear to compressional velocity decrease persists. Similar results were obtained from *PdP* phases of South American and western Pacific earthquakes recorded in California [*Revenaugh and Meyer*, 1997]. Note that the absolute values of the velocity drops are not well constrained by this simple modeling approach, and require a more sophisticated waveform modeling approach such as that taken by *Mori and Helmberger* [1995]. Adopting δV_P=-10% [*Mori and Helmberger*, 1995], consistent with *SPdKS* modeling, suggests shear velocity drops of 25 to 40% when we average our stacks of all regions [see *Revenaugh and Meyer*, 1997]. These numbers are in excellent agreement with predictions for a partial melt layer [*Williams and Garnero*, 1996].

3.4 PKP Data

As with *PcP* data, strong contrasts in seismic properties at the top of the ULVZ (including shear velocity) can affect *PKP* waves, giving rise to precursors [*Vidale and Hedlin*, 1998; *Wen and Helmberger*, 1998a]. In fact, in the southwest Pacific, anomalously large *PKP* precursor amplitudes have been attributed to small scale heterogeneity with 10 to 15% RMS V_P variations over a 60 km layer, having an origin of partial melt [*Vidale and Hedlin*, 1998]. *P* heterogeneity of 8% RMS with an 8 km correlation length was given by *Wen and Helmberger* [1998a], with identical implications. Thus future work analyzing and modeling *PKP* precursors on a global scale holds promise for further ULVZ characterization.

4. ULVZ MODELING TRADE-OFFS

Past modeling efforts have mapped V_P reductions in the ULVZ of 10% [e.g., *Garnero and Helmberger*, 1996]. Subsequently, *Williams and Garnero* [1996] predicted that associated V_S reductions should be on the order of 30%, if the origin of the ULVZ is partial melt. The *PdP-PcP* modeling of *Revenaugh and Meyer* [1997] appears to corroborate such 3:1 δV_S:δV_P reductions. In order to accommodate the effects on *SPdKS-SKS* timing of such a large V_S drop and still explain the observations, *Garnero and Helmberger* [1998] showed that the ULVZ layer thickness must be reduced by approximately one-half of that in *Garnero and Helmberger* [1996], i.e., a ULVZ maximum thickness of 20 kilometers as compared to 40 kilometers. Also, large density (ρ) increases in the ULVZ can retard the peak time of the *SPdKS* arrival, by increasing the amplitude of the internal reflection (*SpKS*, Figure 1b), leading to further reduction of modeled ULVZ layer thickness [*Garnero and Helmberger*, 1998].

Trade-offs in modeling a given *SPdKS* record are schematically illustrated in Figure 7. The shape of the solution space is represented as a plane, but may more appropriately be a volume (possibly with curvature) given uncertainties in the data. This figure can be used to make several important points. First, there exists a minimum ULVZ velocity reduction (and associated thickness) that can explain any given anomaly. This is especially apparent in those data with very short *Pd* segments in *SPdKS* that have several second anomalies, e.g., to model a 4 s *SPdKS* delay accrued over a 100 kilometers *Pd* segment requires a minimum V_P reduction of around 10%. Predictions for models having milder reductions over a thicker layer are unable to explain the anomalous data. As the figure shows, greater velocity reductions can be accommodated for smaller ULVZ thicknesses. Thus the trade-off goes in the direction of thinner boundary layers with more extreme contrasts in properties. If density is allowed to increase, as might be expected for iron enrichment, then ULVZ thickness is reduced. We

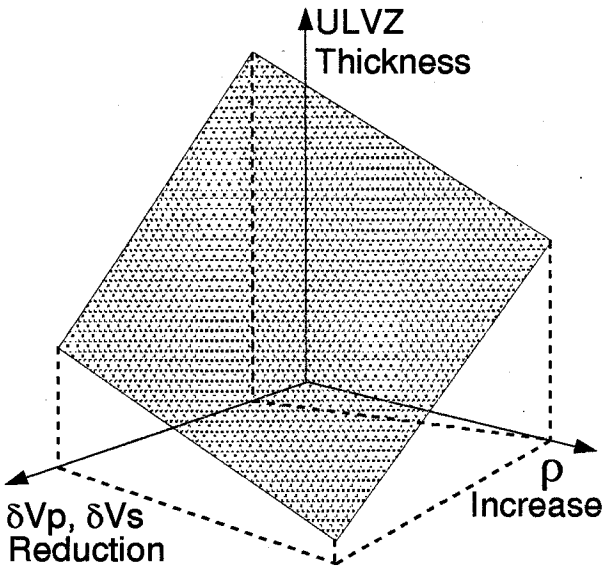

Figure 7. Schematic illustration showing trade-offs in *SPdKS* modeling space. Larger ULVZ velocity reductions can be accommodated if layer thickness is reduced. Increasing density in the ULVZ layer must also be accompanied with a layer thickness reduction (see text for more details).

note that large density increases (e.g., ≥50%) with no associated velocity reductions can produce *SPdKS* anomalies, due to increasing the *SpKS* amplitude. The actual scales on the axes in Figure 7 depend on the record being modeled, as well as on the δV_S:δV_P ratio assumed. Modeling distance profiles of seismic data, including analyses of different phases sampling the same region, help to reduce these trade-offs. Uncertainties in ULVZ modeling are many, but some bounds can be placed on maximum thickness, minimum velocity reduction, and their variations [*Garnero and Helmberger*, 1998].

SPdKS modeling typically assumes a sharp discontinuity at the top of the ULVZ. While this is supported by observation of short period *PdP* [*Mori and Helmberger*, 1995; *Revenaugh and Meyer*, 1997], the depth interval over which the change in properties occurs from the ULVZ to the overlying mantle certainly requires further analysis.

5. MINERAL PHYSICS CONSIDERATIONS

Constraints on the physical origins of the ULVZ can be derived from the families of solutions for the *P*- and *S*-wave velocities and density within such a layer (e.g., see Figure 7). From the available seismic constraints, it is apparent that the ULVZ is remarkable in at least two major respects. First, the negative sign of the *P*- and *S*-velocity changes implies the ULVZ is fundamentally different from most other mantle discontinuities, with only the "low velocity zone" and the actual core-mantle boundary having similar characteristics. We do not view it as coincidence that each of these other boundaries has either been proposed to be produced by partial melting or, for the CMB, is due to both melting and a profound change in chemistry. The second notable aspect of the ULVZ is the magnitude of its velocity contrasts. These exceed those present at any other horizontal boundary in the planet aside from the surface and the CMB (Figure 8). The absolute change in V_P is about a factor of two greater than that observed at the seismic discontinuities observed near 400 and 670 kilometers depth. The inferred V_S discontinuity associated with the ULVZ dwarfs those present at the major mantle discontinuities (including the that at the top of D″) by a factor of five or more. As a result, it appears that the ULVZ is the largest seismic anomaly in the mantle, with shifts in seismic velocity more reminiscent of a magma chamber than those generally associated with simple changes in phase or moderate alterations in chemistry. Again, we do not view this similarity between the properties of the ULVZ and those of partially molten systems as coincidental [e.g., *Williams and Garnero*, 1996]. However, because of the considerably different phases and chemical behavior which exist at the ultra-high pressure and temperature conditions of D″ relative to the uppermost mantle conditions, it is important to evaluate different mechanisms that might give rise to such a basal layer.

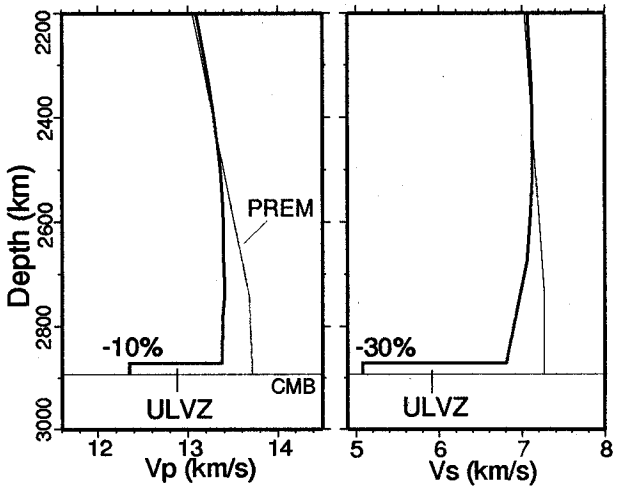

Figure 8. Lower mantle velocity profiles, displaying a ULVZ with 10% V_P and 30% V_S reductions, 2-3% reductions in D″ above the ULVZ is also shown. These profiles are characteristic of the Pacific region, where there are reduced velocities in the lowermost several hundred kilometers of the mantle overlying the ULVZ.

The primary mechanisms for generating a layer at the base of the mantle (or indeed, anywhere in the mantle) are through a change in chemistry and/or a change in phase at depth: in the case of melting, these options obviously need not be exclusive. Several mechanisms exist which could alter the chemistry of the mantle at depth: these include *i)* enrichment in material associated with subduction (whether formerly basaltic crust or its complementary harzburgitic material [*Christensen and Hofmann*, 1994]; *ii)* core-mantle boundary reaction products [*Knittle and Jeanloz*, 1989, 1991]; and *iii)* negatively buoyant descent of melt from the overlying lower mantle [e.g., *Rigden et al.*, 1984]. The first of these options is unlikely to explain the magnitude of ULVZ velocity anomalies without the occurrence of large-scale melting. Harzburgite, which is expected to be enriched in $(Mg,Fe)_2SiO_4$, should have rather similar elastic behavior to the lower mantle; similarly, the primary mineralogic difference between subducted basalt and an approximately peridotitic mantle is in the increased calcium and aluminum (and, to a lesser degree, iron) content of the basalt. Therefore, any material of basaltic chemistry is expected to contain relatively large amounts of $CaSiO_3$-perovskite. From the known elastic behavior of silicate perovskites, it appears that $CaSiO_3$-perovskite is nearly indistinguishable in elastic properties from magnesium silicate perovskite-rich assemblages [e.g., *Mao et al.*, 1989], demonstrating it is extremely unlikely that calcium enrichment could generate the very large difference in seismic properties observed in the ULVZ. The role of aluminum in altering the elastic properties of the silicate perovskites is ill-constrained, but densely packed aluminous phases (such as Al_2O_3) tend to have elastic properties which lie generally close to silicate perovskite [*Gieske and Barsch*, 1968; *Bass*, 1995; *Knittle*, 1995].

Williams and Garnero [1996] have calculated the seismic velocity contrast associated with core-mantle boundary reactions, and found that a maximum V_P depression of about 4% can be produced from the mixture which results from such reactions: far short of that necessary to generate the ULVZ. However, if segregation of solid FeO or FeSi occurs from the pure $MgSiO_3$-perovskite and SiO_2 produced by such core-mantle boundary reactions [e.g. *Manga and Jeanloz*, 1996], a nearly pure FeO or FeSi enriched layer could have V_P anomalies which approach 10%. Using parameters from *Williams and Garnero* [1996], the shear velocity anomaly associated with such a layer would be slightly over 20%. Ignoring dynamical issues associated with invoking a relatively dense ULVZ, we note that the V_S anomaly of such a solid FeO/FeSi layer is anticipated to fall short of that implied by Figure 6. This does not preclude the ULVZ from being significantly iron-enriched, potentially through CMB reactions: as *Ito et al.* [1995] have demonstrated, chemical reactions between liquid silicates and iron occur quite readily.

To explain the ULVZ utilizing solid->solid phase transitions requires that dramatic decreases in shear modulus occur across (or associated with) the transition. Indeed, a 30% decrease (or more) in shear wave velocity in this zone implies (if constant density is assumed) that the shear modulus of this layer is approximately half that of the overlying material. Therefore, transitions which involve a softening of the shear modulus provide particularly attractive explanations for low velocity features. However, the primary transition which has been proposed to involve shear softening under CMB conditions is the shift from the stishovite structure of SiO_2 to the $CaCl_2$ structure [*Cohen*, 1992]. Such shear softening typically occurs in the low pressure phase, prior to the occurrence of the phase transition. If the stishovite -> $CaCl_2$ transition in SiO_2 actually generates the ULVZ, a large abundance of SiO_2 at depth (of order 30%) would be required, which necessitates essentially complete breakdown of the silicate perovskites under deep mantle conditions to their constituent oxides. As no compelling seismic evidence exists for a mid-lower mantle discontinuity in material properties that could be associated with the dissociation of silicate perovskite, SiO_2-dependent scenarios for generating the ULVZ require *i)* a dramatic change in mineralogy at depth in the lower mantle; *ii)* the intersection of the Clapeyron slope of the stishovite -> $CaCl_2$ transition with the conditions of the lowermost mantle; and *iii)* a smearing out of the shear softening produced by this transition over the lowermost portion of the mantle, with relatively little (high shear velocity) $CaCl_2$-structure generated at ULVZ depths.

In contrast to the restrictive conditions required for generating the ULVZ via mineralogic or chemical mechanisms, partial melting provides a rather natural means for explaining this feature [*Williams and Garnero*, 1996]. The ability of differing geometry-dependent amounts of partial melts to explain the velocity perturbations associated with the ULVZ are shown in Figure 9. The advantages of partial melting in explaining the ULVZ include *i)* quantitative agreement with large V_P and V_S depressions; *ii)* explanation of why this feature is generally correlated with zones of hot upwelling in the overlying mantle; and *iii)* providing both thermally-based and density-based rationales for this region lying at the absolute base of the mantle. The density of basic melts at ultra-high pressures is anticipated to be either comparable or exceed that of their coexisting solids [*Rigden et al.*, 1984; 1989]. Therefore, if melting is initiated at depth, the melt is likely to either be produced at, or descend to, the base of the mantle. Thus, the partial melting scenario involves a minimum of required special circumstances, but also involves a number of first order uncertainties: these include the geometry of melt distribution, and thus the melt fraction, and the precise chemistry of the melt.

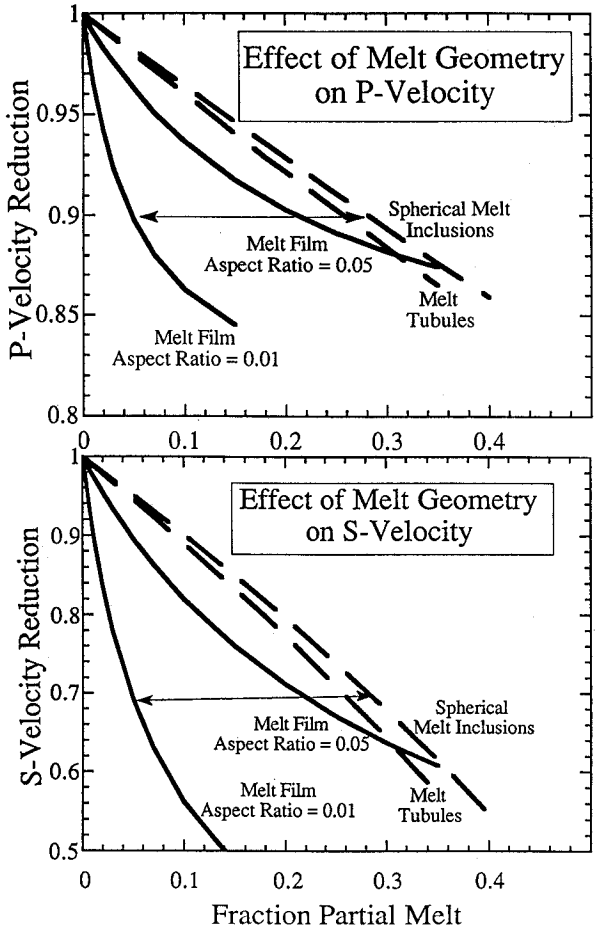

Figure 9. (a) The ratio of *P* wave velocity of melt bearing mantle to that of solid mantle for varying melt fractions and geometries. Arrow indicates the range of melt fractions that produce a 10% V_P reduction. (b) As in (a), except for shear waves. Arrow corresponds to the variation in melt fraction implied by the inferred 10% V_P depression, coupled with results of (a). [After *Williams and Garnero*, 1997.]

6. GEODYNAMICS CONSIDERATIONS

The existence of a thermal boundary layer at the base of the mantle is quite probable [*Stacey and Loper*, 1983], with the hottest temperatures in the mantle existing just above the core. The temperature increase in the CMB thermal boundary layer is uncertain, but has been estimated by comparing mantle adiabats and core melting temperatures to be on the order of 800° or more [e.g., *Jeanloz and Morris*, 1986] The increase in temperature with depth into the thermal boundary layer provides a natural mechanism for concentrating partial melt in a ULVZ, especially if densities are elevated. The deepest part of the boundary layer will be the lowest viscosity region as well, with strong horizontal flows being likely. The CMB is essentially isothermal due to the low viscosity of the core, thus a ULVZ might be globally present if it represents partial melting of a bulk component of the lower mantle (such as MgO). However, regions with mantle downwellings should have thinner thermal boundary layers than regions with upwellings, due to dynamical effects on a low viscosity basal layer and also radial temperature gradients, giving rise to lateral variations in thickness of the ULVZ. ULVZ thicknesses are at most a few tens of kilometers, and possibly modulated down to unobservable levels beneath regions of cold downwellings. Hotter temperatures early in Earth history could have produced a thicker global ULVZ in this scenario.

A purely thermal cause for the ULVZ, with associated partial melting of some bulk mantle component, predicts interesting dynamical effects that we explore. Survival of the zone of partial melt requires a significant density increase to resist entrainment or upward drainage, especially given the effects of reduced viscosity and probably small-scale convection. In fact, the partially molten region may convect separately from the large scale overlying mantle flow, modifying heat flux out of the core in thick ULVZ regions, resulting in the hottest areas of D″, with small radial thermal gradients. Such enhanced efficiency of heat transport across the CMB could influence core flow as well as mantle upwelling, perhaps increasing the lateral dimension of the latter relative to the concentrated upwelling expected for hot subsolidus boundary layers. Numerical calculations are needed to fully explore these ramifications.

If chemical heterogeneity is also an important factor for the existence of any lateral variations in the ULVZ, the dynamical issues are even more complex. If the origin of the ULVZ is partially (or completely) due to compositional uniqueness relative to the lower mantle, then it must be denser than the lower mantle to be gravitationally stable. Stability is determined by a buoyancy ratio, the ratio of the compositional to thermal buoyancy, $\Delta\rho_{ULVZ}/\rho\alpha\Delta T$ where $\Delta\rho_{ULVZ}$ is the density anomaly of the ULVZ, ρ is the density of the lower mantle, α is the coefficient of thermal expansion, and ΔT is the temperature difference across the layer (see *Hansen and Yuen* [1990] for a detailed discussion of the physics of thermo-chemical convection.) Generally, a buoyancy number close to 1 results in a compositionally distinct layer through time; this corresponds to a minimum increase in $\Delta\rho_{ULVZ}$ of around 6% [*Sleep*, 1988]. Such a layer will pile up under upwellings [*Davies and Gurnis*, 1986]. A large viscosity drop due to partial melt can change this result, as low-viscosity dense material is not as easily entrained in mantle plumes [*Sleep*, 1988].

Several studies have used numerical or laboratory models of thermo-chemical convection to determine the

conditions for maintaining a stable, dense layer, and the structure of that layer [e.g., *Davies and Gurnis* 1986; *Hansen and Yuen*, 1988, 1989; *Olson and Kincaid*, 1991; *Kellogg and King*, 1993]. In time-dependent flow models, a stable layer often forms complex features due to internal circulation and mixing between the dense layer and the overlying layer. The structure of a thermo-chemical boundary layer at the base of the mantle is influenced primarily by the intrinsic density of the layer, but the vigor of the convection throughout the mantle, the rheology within the layer and in the overlying mantle, and the thermal conductivity of the layer relative to the lower mantle also play a role.

The most complex structures are observed when the layer is marginally stable [*Hansen and Yuen*, 1990; *Kellogg and King*, 1993]. At moderate buoyancy ratios (up to about 1), the layer tends to be stable but can vary drastically in thickness from nearly invisible where it has been pushed away by downwellings to relatively thick under upwellings (see Figure 10). As the buoyancy ratio increases, so does the stability of the ULVZ layer, and at higher buoyancy numbers the resulting layer is rather stagnant, not varying much in thickness from place to place [*Kellogg and King*, 1993; *Kellogg*, 1997].

However it originates, a ULVZ layer at the base of the mantle can significantly influence the thermal structure of the lower mantle (especially upwelling plumes) and the heat flux across the CMB. Maintaining a stable ULVZ layer at the base of the convecting mantle results in an increased temperature gradient across the lower boundary layer; hence the temperature at the base of the mantle may be relatively high (Figure 10a). Upwelling mantle plumes in this case may not arise directly from the core-mantle boundary and so one possible consequence of a stable layer at the base of the mantle could be cooler plumes [*Farnetani*, 1997]. An iron-rich layer at the base of the mantle would also be a good heat conductor [*Manga and Jeanloz*, 1996]. The consequences of high heat flow though the ULVZ (and thus D″) layer may also include more stable and hotter plumes [*Manga and Jeanloz*, 1996]. The layer itself may stablize plumes, as piles of dense material provide an "anchor" for upwellings [*Manga and Jeanloz*, 1996; *Montague et al.*, 1996].

The detailed thermal structure of the lower mantle will be determined in part by whether the ULVZ layer circulates internally. In order to attempt answering to this question, we must estimate the Rayleigh number in this layer. In principle, if the Rayleigh number is supercritical, we would expect that the layer is convecting internally. However, uncertainties in important ULVZ properties, such as ΔT across the layer, and viscosity preclude any constrained estimate of the Rayleigh number at present. Thus we cannot rule out free convection; nor can we assert that there must be vigorous convection within the layer. The flow patterns within the layer may be strongly influenced by the overall pattern of circulation within the lower mantle. Convection within a thick ULVZ may result in an additional thermal boundary layer at both the base and the top of the ULVZ (Figure 10c). On the other hand, the steep thermal gradient at the base of the mantle might account for the ULVZ.

7. DISCUSSION

We now compare the ULVZ distribution of Figure 1 to various other geophysical phenomena. Figure 11a shows the distributions of buoyancy flux weighted hot spots (white circles, from *Sleep* [1992]) and calculated locations of subducted material in the D″ layer (crosses, from *Lithgow-Bertelloni and Richards* [1998]) superimposed on the ULVZ map. The hot spot spatial pattern is correlated with the pattern of ULVZ detections. For the hotspot catalog of Sleep (1990), the probability of chance correlation exceeding the observed is ~1%. When hotspots are weighted by flux (Sleep, 1990), the likelihood of chance correlation drops to 0.37% [*Williams et al.*, 1998]. Also evident in the figure, is that projected locations of subducted material most strongly coincide with areas where a ULVZ has not been detected, as well as where hot spots are absent (as expected in regions of downwelling, e.g., see *Richards and Engebretson* [1992]). This suggests thermal and/or dynamical effects on ULVZ structure and distribution from overlying convection.

A partially molten iron rich layer can have higher electrical conductivity [e.g., see *Jeanloz*, 1990]. Therefore the presence of a ULVZ potentially influences the Earth's magnetic field. Figure 11b shows magnetic field reversal paths and ULVZ distribution The calculated distribution of reversal paths are most strongly correlated

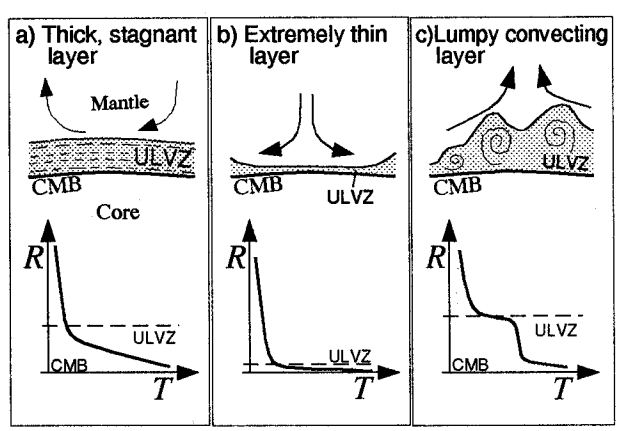

Figure 10. Schematic cross-sections and temperature profiles for (a) a thick stagnant ULVZ layer; (b) an extremely thin ULVZ; and (c) a thick, contorted convecting ULVZ layer (vertical dimension exaggerated).

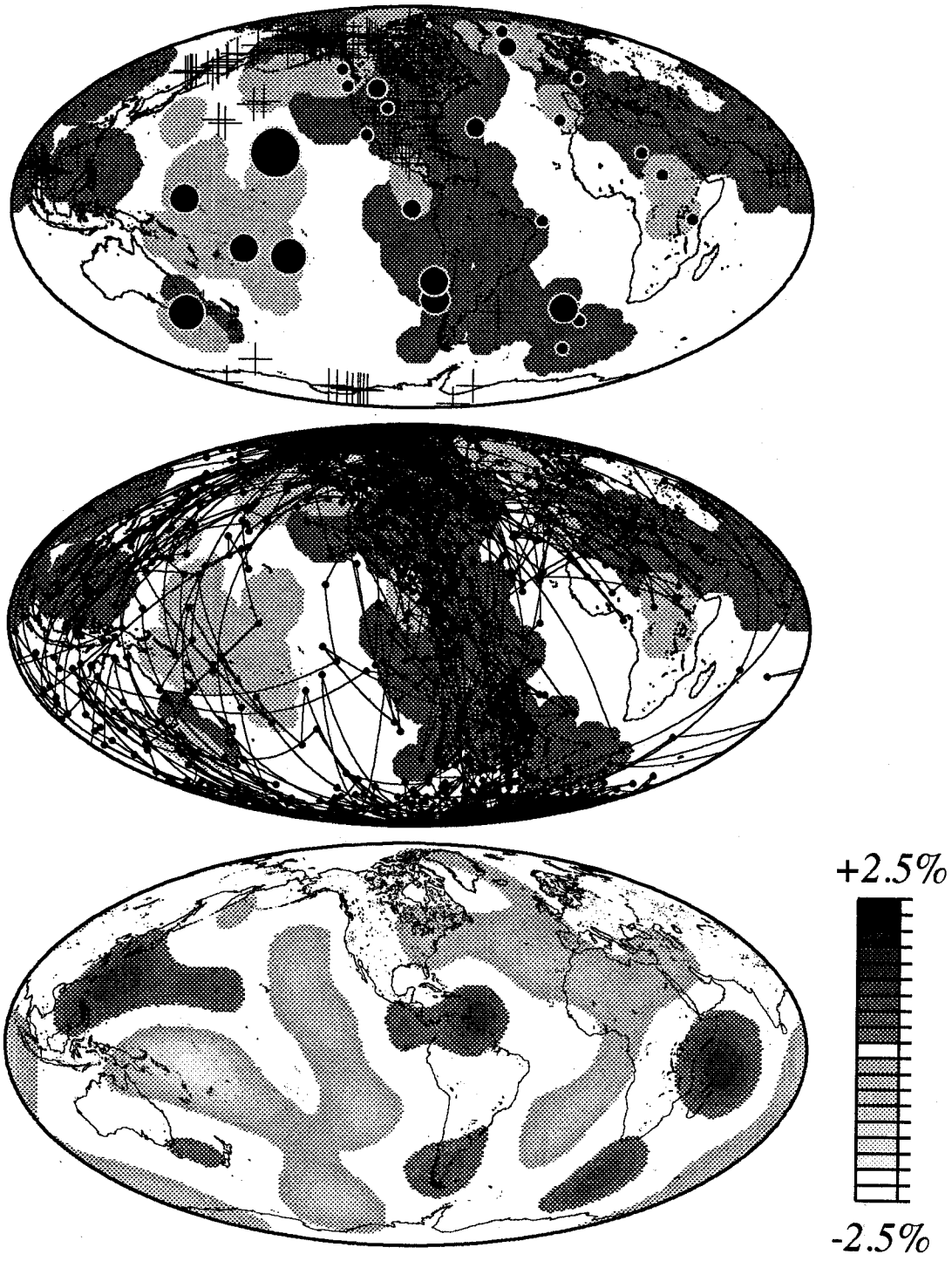

Figure 11. Mollweide projection of globe showing: (top) ULVZ distribution as in Figure 1: light shading corresponds to Fresnel zone regions where a ULVZ has been detected, dark regions are where no ULVZ is detected, no shading corresponds to no coverage. Black-filled circles are hot spot locations (where we have ULVZ coverage), scaled to buoyancy flux estimates of *Sleep* [1992]. Crosses are locations of calculated lower mantle density anomalies due to subducted material [*Lithgow-Bertelloni and Richards*, 1998]. (middle) ULVZ distribution with VGP reversal paths of *Laj et al.* [1991]. (bottom) *P* wave velocity heterogeneity in the lowermost 200-300 kilometers of the mantle, as calculated by *Wysession* [1996a]. Light and dark regions correspond to low and high velocity perturbations, respectively, with the ±0.5% range padded white.

with regions where a ULVZ has not been detected (e.g., under South and North America). If the ULVZ is iron-rich, and has relatively high electrical conductivity, regions where the ULVZ is thick and easily detected may be avoided by the poles of the magnetic field during reversals [e.g., see *Aurnou et al.*, 1996].

A recent inversion for large scale V_P structure in the lowermost few hundred km of the mantle is presented in Figure 11c for comparison the ULVZ distribution [from *Wysession*, 1996b]. High and low velocities (dark and light shadings, respectively) outside the $-0.5\% < \delta V_P < 0.5\%$ range are contoured. In most of the areas studied, the ULVZ is present in regions of large scale *P* velocity reductions (Figure 11c). However, some areas lack this correlation, such as under parts of northern Africa, off the west coast of Central America, or just off the east coast of Japan. This may be the result of poor resolution in the tomographic image due to the long D″ paths of the *Pd* phase used in that study. On the other hand, the depth scales sampled by ULVZ investigations and lower mantle tomography studies are quite different (i.e., 5-40 kilometers compared to 200-400 kilometers, respectively), and thus may be sampling different length scales that need not be strongly correlated spatially. Alternatively, we cannot preclude a thin ULVZ (< 5 km) in these regions, which might go undetected by the long-period WWSSN data.

The large scale low-velocity feature in the southwest Pacific [e.g., see *Su et al.*, 1994; *Wysession*, 1996b; *Masters et al.*, 1996] has been interpreted as a large scale lower mantle thermal upwelling (often referred to as a "superplume"), and coincides with a large ULVZ patch. A ULVZ that laterally extends over a large area may act as the source to many plumes (and thus hot spots), which may effectively heat the lower mantle over large scale lengths, giving rise to low seismic velocities at long wavelengths. However, inversions at shorter scale lengths, such as that of *Grand et al.* [1997], show more variability in the southwest Pacific D″ structure, with alternating high and low velocities. Future investigations should attempt to resolve to what extent previous superplume interpretations are dependent upon scale length of resolvability, as well as spatial correlation of reduced lower mantle velocities and ULVZ distribution. *Lay et al.* [1997] detect significant small scale heterogeneities within the D″ layer in circum-Pacific regions, thus an intermittent ULVZ in these regions may be a possibility.

As previously mentioned, analyses of seismic phases other than *SPdKS* and precursors to core reflected energy may not show direct evidence for ULVZ structure, especially considering the strong ULVZ lateral variations [*Garnero and Helmberger*, 1996, 1998]. Long range diffracted energy, however, can allow us to place constraints on ULVZ structure allowable in any average structure. In an analysis of broadband amplitudes, travel times, and waveforms of diffracted shear waves *Ritsema et al.* [1997] show that a ULVZ can be tolerated in a one-dimensional reference structure for the region beneath the central Pacific if ULVZ thickness is $\leq$ 5 km (assuming δV_P=-10% and δV_S=-30%). Lateral variations with much thicker localized ULVZ regions [as in *Garnero and Helmberger*, 1996] cannot be precluded by the data. Intense small scale lateral variations in ULVZ topography and/or heterogeneity [*Wen and Helmberger*, 1998; *Helmberger et al.*, 1998; *Garnero and Helmberger*, 1998] can however give rise to spatial patterns in the amplitudes of *PKP* precursor energy correlating with the ULVZ distribution [see *Vidale and Hedlin*, 1998]. Future seismological efforts should include predictions through more detailed ULVZ structures, such as variable ULVZ topography [as in *Wen and Helmberger*, 1998b].

It is possible that systematic layering of ULVZ melt material, either solidified or liquid, may be related to the cause of D″ anisotropy [see *Lay et al.*, 1998]. A better understanding of lower mantle mineralogy along with more detailed seismic information are necessary to establish the feasibility of such a scenario. Future ULVZ modeling must include exploring the whole parameter space of ULVZ thickness, V_P, V_S, ρ, as well as possible strong attenuation due to partial melt, to determine the range of acceptable models, which will ultimately help in determining plausible ULVZ as well as lowermost mantle mineralogy.

8. CONCLUSIONS

Evidence for a thin boundary layer of ultralow velocities is provided by several seismic phases analyzed by different methods. The resulting distribution of ULVZ layering, where we have coverage, correlates strongly with hot spot locations (especially flux-weighted hot spots) and lower mantle velocity reductions. Regions where a ULVZ has not been detected (therefore, absent or thinner than our 3-5 kilometers threshold of detection thickness) spatially correlate to predicted locations of subducted slab material, higher seismic velocities in the overlying mantle, as well as virtual geomagnetic pole reversal paths. The preferred explanation of the cause of the ULVZ is partial melting of lowermost mantle rock, with probable chemical variations (e.g., from core-mantle chemical reaction products) producing very short wavelength heterogeneity. The emerging picture is thus one in which the layering in the lowermost mantle is strongly coupled to the dynamics of mantle circulation: low viscosity partially molten ULVZ regions may support elevated heat flow from the core, forming the root of mantle plumes; and such a layer is suppressed in regions where cold downwelling material has fallen to the CMB. The hypothesis of extensive material exchange between the upper and lower mantles is strongly supported by this ULVZ analysis.

Acknowledgements. We thank Carolina Lithgow Bertelloni for the lower mantle slab calculations, Michael Wysession for the lower mantle V_P model, Daniel Brito for the paleomagnetic reversal paths, Julie Zaslow and Xiaoming Ding for data, and the authors of GMT software with which all figures were constructed [*Wessel and Smith*, 1991]. Thanks also to Steve Grand, Don Helmberger, Barbara Romanowicz, and John Vidale for helpful discussions. Also, reviews by M. Wysession and an anonymous reviewer improved the manuscript. Contribution #334 of the W. M. Keck Seismological Laboratory and Institute of Tectonics. This research was partially supported by NSF grant EAR9305894. E.J.G. was supported by NSF grant EAR-9896046 and EAR9418643. Workshops on the core-mantle boundary organized under EAR9305894 were instrumental in developing interdisciplinary coordination on this topic. The 1996 Fall AGU Meeting held a special session on the core-mantle boundary that further focussed attention on this topic.

9. REFERENCES

Aurnou, J.M., J.L Buttles, G.A., Neumann, and P.L. Olson, Electromagnetic core-mantle coupling and paleomagnetic reversal paths, *Geophys. Res. Lett., 23,* 2705-2708, 1996.

Bass, J.D., Elasticity of minerals, glasses and melts, Handbook of Physical Constants, Vol. 2, pp. 45-63, Ed. T.J. Ahrens, American Geophysical Union, Washington, D.C., 1995.

Choy, G. L., Theoretical seismograms of core phases calculated by frequency-dependent full wave theory, and their interpretation, *Geophys. J. R. astr. Soc., 51,* 275-312, 1975.

Christensen, U.R., and A.W. Hofmann, Segregation of subducted oceanic crust in the convecting mantle, *J. Geophys. Res., 99,* 19867-19884, 1994.

Cohen, R.E., First principles predictions of elasticity and phase transitions in high pressure SiO_2 and geophysical implications, in High Pressure Research: Application to Earth and Planetary Sciences, Eds. Y. Syono and M.H. Manghnani, pp. 425-431, American Geophysical Union, Washington, D.C., 1992.

Davies, G.F., and M. Gurnis, Interaction of mantle dregs with convection: lateral heterogeneity at the core-mantle boundary, *Geophys. Res. Lett., 13,* 1517-1520, 1986.

Doornbos, D. J., and T. Hilton, Models of the core-mantle boundary and the travel times of internally reflected core phases, *J. Geophys. Res., 94,* 15,741-15,751, 1989.

Dziewonski, Mapping the lower mantle: Determination of lateral heterogeneity in *P* velocity up to degree and order 6, *J. Geophys. Res., 89,* 5929-5952, 1984.

Dziewonski, A. M., and D. L. Anderson, Preliminary reference Earth model (PREM), *Phys. Earth Planet. Int., 25,* 297-356, 1981.

Farnetani, C.G., Excess temperature of mantle plumes; The role of chemical stratification across D″, *Geophys. Res. Lett., 24,* 1583-1586, 1997.

Fischer, K.M., J.M. Zaslow, E.J.Garnero, M.J. Fouch, M.E. Wysession, T.J. Clarke, and G.I. Al-eqabi, SpdKS constraints on a thin slow layer at the base of the mantle beneath the northwestern Pacific, *Eos Trans. AGU, 77,* no. 48, 1996.

Fuchs, K. and G. Müller, Computation of synthetic seismograms with the reflectivity method and comparison with observations, *Geophys. J. R. Astron. Soc., 23,* 417-433, 1971.

Garnero E. J., S. P. Grand, and D. V. Helmberger, Low *P* wave velocity at the base of the mantle, *Geophys. Res. Lett., 20,* 1843-1846, 1993.

Garnero, E.J., and D.V. Helmberger, Seismic detection of a thin laterally varying boundary layer at the base of the mantle beneath the central-Pacific, *Geophys. Res. Lett., 23,* 977-980, 1996.

Garnero, E.J., and D.V. Helmberger, Further constraints and uncertainties in modeling a thin laterally varying ultralow velocity layer at the base of the mantle, *J. Geophys. Res.* (in press), 1998.

Gieske, J.H., and G.R. Barsch, Pressure dependence of the elastic constants of single crystalline aluminum oxide, *Physica Status Solidi, 29,* 121-31, 1968.

Grand, S.P., R.D. van der Hilst, and S. Widiyantoro, Global seismic tomography: a snapshot of convection in the Earth, *G.S.A. Today, 7,* 1-7, 1997.

Hansen, U, and Yuen, D.A., Numerical simulations of thermal-chemical instabilities at the core-mantle boundary, *Nature, 334,* 237-240, 1988.

Hansen, U, and Yuen, D.A., Dynamical influences from thermal-chemical instabilities at the core-mantle boundary, *Geophys. Res. Lett., 16,* 629-632, 1989.

Hansen, U. and Yuen, D.A., Nonlinear physics of double-diffusive convection in geological systems, *Earth-Sci. Rev., 29,* 385-399, 1990.

Helmberger, D.V., E.J. Garnero, and X.-M. Ding, Modeling two-dimensional structure at the core-mantle boundary, *J. Geophys. Res., 101,* 13,963-13,972, 1996.

Helmberger, D.V., L. Wen, and X. Ding, Ultra low velocity zone beneath Iceland, *Nature,* (in review) 1998.

Holland, K.G., and T.J. Ahrens, Melting of $(Mg,Fe)_2SiO_4$ at the core-mantle boundary of the Earth, *Science, 275,* 1623-1625, 1997.

Inoue H., Y. Fukao, K. Tanabe, and Y. Ogata, Whole mantle *P* wave travel time tomography, *Phys. Earth Planet. Int., 59,* 294-328, 1990.

Ito, E., K. Morooka, O. Ujike and T. Katsura, Reactions between molten iron and silicate melts at high pressure: Implications for the chemical evolution of Earth's core, *J. Geophys. Res., 100,* 5901-5910, 1995.

Jeanloz, R., The nature of the Earth's core, *Ann. Rev. Earth Planet. Sci., 18,* 357-386, 1990.

Jeanloz, R., and S. Morris, Temperature distribution in the crust and mantle, *Ann. Rev. Earth Planet. Sci., 14,* 377-415, 1986.

Kellogg, L.H. and S.D. King, Effect of mantle plumes on the growth of D″ by reaction between the core and mantle, *Geophys. Res. Lett., 20,* 379-382, 1993.

Kellogg, L.H., Growing the Earth's D″ layer: Effect of density variations at the core-mantle boundary, *Geophys. Res. Lett., 24,* 2749-2752, 1997.

Knittle, E., Static compression measurements of equations of state, Handbook of Physical Constants, Vol. 2, pp. 98-142, Ed. T.J. Ahrens, American Geophysical Union, Washington, D.C., 1995.

Knittle, E. and R. Jeanloz, Simulating the core-mantle boundary: an experimental study of high-pressure reactions between silicates and liquid iron, *Geophys. Res. Lett., 16,* 609-612, 1989.

Knittle, E. and R. Jeanloz, Earth's core-mantle boundary: results of experiments at high pressures and temperatures, *Science, 251*, 1438-1443, 1991.

Krüger, F., M. Weber, F. Scherbaum, and J. Schlittenhardt, Normal and inhomogeneous lowermost mantle and core-mantle boundary structure under the Arctic and northern Canada, *Geophys. J. Int., 122*, 637-658, 1995.

Laj, C., A. Mazaud, R. Weeks, M. Fuller, and E. Herrero-Berverra, Geomagnetic reversal paths, *Nature, 351*, 447, 1991.

Lay, T., E.J. Garnero, C.J. Young, and J.B. Gaherty, Scale lengths of shear velocity heterogeneity at the base of the mantle from *S* wave differential travel times, *J. Geophys. Res., 102*, 9887-9909, 1997.

Lay, T., E.J. Garnero, Q. Williams, R. Jeanloz, B. Romanowicz, L. Kellogg, and M.E. Wysession, Shear wave anisotropy in the D″ region and its implications, AGU Geophysical Monograph on the Core-Mantle Region, (this volume) 1998.

Lithgow-Bertelloni, C., and M.A. Richards, The dynamics of cenezoic and mesozoic plate motions, *Ann. Rev. Earth Planet. Sci., 36*, 27-78, 1998.

Loper, D.E., and T. Lay, The core-mantle boundary region, *J. Geophys. Res., 100*, 6397-6420, 1995.

Manga, M. and Jeanloz, R. Implications of a metal-bearing chemical boundary layer in D″ for mantle dynamics, *Geophys. Res. Lett., 23*, 3091-3094, 1996.

Mao, H.K., Chen, L.C., Hemley, R.J., and A.P. Jephcoat, Stability and equation of state of CASiO3-perovskite to 134-GPA, *J. Geophys. Res., 94*, 17889-17894, 1989.

Montague, M., M. Manga, L.H. Kellogg, R. Jeanloz, Models of a metal-bearing chemical boundary layer in the D″ region: Implications for mantle and core dynamics, *EOS, Trans. AGU, 77*, 709-710, 1996.

Mori, J., and D.V. Helmberger, Localized boundary layer below the mid-Pacific velocity anomaly identified from a *PcP* precursor, *J. Geophys. Res., 100* 20,359-20,365, 1995.

Olson, P. and C. Kincaid, Experiments on the interaction of thermal convection and compositional layering at the base of the mantle, *J. Geophys. Res., 96*, 4347-4354, 1991.

Pulliam, R.J., D.W. Vasco, and L.R. Johnson, Tomographic inversions for mantle *P* wave velocity structure based on the minimization of l^2 and l^1 norms of International Seismic Centre travel time residuals, *J. Geophys. Res., 98*, 699-734, 1993.

Revenaugh J.S., and R. Meyer, Seismic evidence of partial melt within a possibly ubiquitous low-velocity layer at the base of the mantle, *Science, 277*, 670-673, 1997.

Richards, M.A., and D.C. Engebretson, Large-scale mantle convection and the history of subduction, *Nature, 355*, 437-440, 1992.

Rigden, S.M., T.J. Ahrens, and E.M. Stolper, Densities of liquid silicates at high pressures, *Science, 226*, 1071-1074, 1984.

Rigden, S.M., T.J. Ahrens, and E.M. Stolper, High-pressure equation of state of molten anorthite and diopside, *J. Geophys. Res., 94*, 9508-9522, 1989.

Ritsema, J.E., E.J. Garnero, and T. Lay, A strongly negative shear velocity gradient and lateral variability in the lowermost mantle beneath the Pacific, *J. Geophys. Res, 102*, 20,395-20,411, 1997.

Scherbaum, F., F. Krüger, and M. Weber, Double beam imaging: mapping lower mantle heterogeneities using combinations of source and receiver arrays, *J. Geophys. Res., 102*, 507-522, 1997.

Silver, P., and C. R. Bina, An anomaly in the amplitude ratio of *SKKS/SKS* in the range 100-108° from portable teleseismic data, *Geophys. Res. Lett., 20*, 1135-1138, 1993.

Sleep, N.H., Gradual entrainment of a chemical layer at the base of the mantle by overlying convection, *Geophys. J., 95*, 437-447, 1988.

Sleep, N.H., Time dependence of mantle plumes: some simple theory, *J. Geophys. Res., 97*, 20,007-20,019, 1992.

Song, X.-D., and D.V. Helmberger, A *P* wave velocity model of Earth's core, *J. Geophys. Res., 100*, 9817-9830, 1995.

Souriau, A., and G. Poupinet, Lateral variations in *P* velocity and attenuation in the D″ layer, from diffracted *P* waves, *Phys. Earth Planet. Int., 84*, 227-234, 1994.

Sylvander, M. and A. Souriau, Mapping S-velocity heterogeneities in the D″ region, from *SmKS* differential travel times, *Phys. Earth Planet. Int., 94*, 1-21, 1996.

Sylvander, M., B. Ponce, and A. Souriau, Seismic velocities at the core-mantle boundary inferred from P waves diffracted around the core, *Phys. Earth Planet. Int., 101*, 189-202, 1997.

Stacey, F.D. and D.E. Loper, The thermal boundary-layer interpretation of D″ and its role as a plume source, *Phys. Earth Planet. Int., 33*, 45-55, 1983.

Su, W.-J., R.L. Woodward, and A.M. Dziewonski, Degree 12 model of shear velocity heterogeneity in the mantle, *J. Geophys. Res., 99*, 6945-6980, 1994.

Vidale, J.E., and M.A.H. Hedlin, Intense scattering at the core-mantle boundary north of Tonga: evidence for partial melt, *Nature* (in press), 1998.

Vidale, J.E., E.J. Garnero, and L.S.L. Kong, Sounding the base of the mantle by core reflections, *Eos Trans. AGU, 76*, no. 46, 404, 1995.

Weber, M., *P* and *S* wave reflections from anomalies in the lowermost mantle, *Geophys. J. Int., 115*, 183-210, 1993.

Weber, M., and M. Körnig, Lower mantle inhomogeneities inferred from *PcP* precursors, *Geophys. Res. Lett., 17*, 1993-1996, 1990.

Wen, L., and D.V. Helmberger, Ultra low velocity zones near the core-mantle boundary from broadband *PKP* precursors, *Science*, (in press) 1998a.

Wen, L., and D.V. Helmberger, A 2-D P-SV hybrid method and its application to modeling localized structures near the core-mantle boundary, *J. Geophys. Res.*, (in press) 1998b.

Williams, Q., and E.J. Garnero, Seismic evidence for partial melt at the base of Earth's mantle, *Science, 273*, 1528-1530, 1996.

Williams, Q., J. Revenaugh, and E.J. Garnero, A correlation between the hot spot distribution and ultra-low basal velocities in the mantle, *Nature*, (in review), 1998.

Wysession, M. E., Imaging cold rock at the base of the mantle: The sometimes fate of slabs?, in *Subduction: Top to Bottom*, edited by G.E. Bebout, D. Scholl, S. Kirby, and J.P. Platt, AGU, Washington, D.C., pp. 369-384, 1996a.

Wysession, M. E., Large-scale structure at the core-mantle boundary from diffracted waves, *Nature, 382*, 244-248, 1996b.

Wysession, M. E., and E. A. Okal, Regional analysis of D″ velocities from the ray parameters of diffracted *P* profiles, *Geophys. Res. Lett., 16*,1417-1420, 1989.

Wysession, M.E., R.W. Valenzuela, A.-N. Zhu, and L. Bartko,

Investigating the base of the mantle using differential travel times, *Phys. Earth Planet. Int.*, *92*, 67-84, 1995.

Wysession, M.E., T. Lay, J. Revenaugh, Q. Williams, E.J. Garnero, R. Jeanloz, L. Kellogg, The D″ discontinuity and its implications, AGU Geophysical Monograph on the Core-Mantle Region, (this volume) 1997.

Young, C. J., and T. Lay, The core shadow zone boundary and lateral variations of the *P* velocity structure of the lowermost mantle, *Phys. Earth Planet. Int.*, *54*, 64-81, 1989.

E. Garnero, Berkeley Seismological Laboratory, University of California, 475 McCone Hall, Berkeley, CA 94720

J. Revenaugh, Q. Williams, and T. Lay, Institute of Tectonics and Earth Sciences Board, University of California, Santa Cruz, CA 95064

L. Kellogg, Department of Geology, University of California, Davis, CA 95616